EPRI

Fracture Toughness Data for Zirconium Alloys

Application to Spent Fuel Cladding in Dry Storage

1001281

Fracture Toughness Data for Zirconium Alloys

Application to Spent Fuel Cladding in Dry Storage

1001281

Technical Progress, January 2001

EPRI Project Manager

A. Machiels

DISCLAIMER OF WARRANTIES AND LIMITATION OF LIABILITIES

This is an EPRI Level 2 report. A Level 2 report is intended as an informal report of continuing research, a meeting, or a topical study. It is not a final EPRI technical report.

ORDERING INFORMATION

CITATIONS

ABSTRACT

A review of the available literature dealing with fracture testing of zirconium alloys was performed. The purpose of the review was to evaluate the available data in order to develop estimates for fracture toughness values that are applicable to spent fuel conditions. The majority of the data was developed using either plane-strain plate specimens or pressure tube curved specimens. Only one paper dealt with LWR cladding geometry using a newly developed test, which is not an ASTM-qualified test.

The examined database includes unirradiated and irradiated materials with fast fluence levels approaching 10^{22}n/cm^2 (E>1MeV), temperatures ranging from room to reactor operating temperatures, and uniformly charged hydrogen concentrations up to 4000 ppm. Although the hydrogen concentrations cover a wide range, the data does not permit the derivation of a functional dependence of fracture toughness on hydrogen concentration because of the differences in hydrogen morphology from corrosion-induced hydrides. Delayed hydride cracking (DHC) fracture data is included in the present study to assess the applicability of DHC mechanisms to spent fuel storage conditions. Moreover, the DHC data includes fracture toughness information (K_{IH}) that can be used for evaluating the effects of radially oriented hydrides, noting that the normal hydride orientation is circumferential.

Using conservative interpretation of the data, fracture toughness estimates are developed for various burnup levels and temperatures. Because of the absence of cladding-specific conditions in the data, such as cladding geometry, plane-stress fracture, corrosion-induced hydrides, etc., the developed fracture toughness estimates are by necessity bounding values.

Finally, the report presents a correlation that relates the fracture toughness to the critical strain energy density. This correlation allows the user to derive fracture toughness values from the stress-strain curve which, for highly irradiated material, can be constructed from readily available properties, namely, the elastic modulus, the yield strength, and the total elongation. The developed correlation has two main uses: validation of the literature values of fracture toughness for application to a specific spent-fuel condition, and the derivation of fracture toughness values where none exist.

CONTENTS

ILLUSTRATIONS

1

INTRODUCTION

The applicable regulations for spent fuel storage are Part 72 of Title 10 of the Code of Federal Regulations (10CFR72) [1], and the present regulatory practices are documented in supporting Standard Review Plans (SRPs) NUREG-1536 [2] and NUREG-1567 [3]. The supporting SRPs sometimes lack the specificity needed by the licensees to satisfy Part 72 requirements, leaving part of the licensing review process to the individual interpretations of NRC staff and consultants. In particular, use of fracture mechanics in NRC reviews would require the licensees to present analyses that demonstrate cladding integrity using fracture toughness as a failure criterion. However, none of the fracture toughness measurements in the literature deal with fuel cladding specific geometry or material conditions. Consequently, the application of existing data to spent fuel becomes subject to the individual interpretation of the user. Therefore, a unified industry-wide approach is required to avoid the state of confusion and controversy that is likely to develop.

Considerable fracture toughness data under delayed hydryde cracking (DHC) conditions have been generated in the literature, and the potential exists for the incorrect application of the data, as a conservative measure, to long-term storage. Under DHC testing, fracture initiation occurs in materials containing radial hydrides. Therefore, the initial fracture toughness (K_{IH}) becomes a measure of the fracture toughness of such materials, and is the absolute lower bound of K_{IC} for any cladding condition. For these reasons, a discussion of DHC in relation to spent fuel storage is both informative and necessary.

The objective of the present paper is to use the literature data to develop estimates for fracture toughness values that can be applied to spent-fuel cladding. Towards that objective, Section 2 gives a brief perspective on the field to help the reader better understand the limitations of the data, and to point out some of the difficulties facing the industry in applying fracture mechanics to fuel cladding. Section 3 summarizes data from the cited references, which, to allow easy access, is also included in the Appendix. Section 4 gives estimates of fracture toughness values recommended for the various irradiation, temperature, and hydriding conditions. Section 5 provides a correlation that relates the fracture toughness to the stored strain energy density that is subject to release upon fracturing. This correlation is used to estimate the fracture toughness from the material's stress-strain curve, which is usually available, or can be easily obtained. The delayed-hydride-cracking (DHC) phenomenon is discussed in Section 6. Section 7 presents the conclusions.

2

GENERAL PERSPECTIVE

Under the assumptions of the classical Linear Elastic Fracture Mechanics (LEFM), K_{IC} is a measure of unstable fracture under small-scale yielding, for which the plane-strain condition becomes the testing requirement. Where the conditions of small-scale yielding cannot be satisfied, such as for thin materials, fracture occurs under plane-stress condition, and J_{IC} becomes the fracture measure.

In practice, one would assume that the dominant mode of fracture is the crack-opening mode, Mode-I, and would calculate the stress intensity factor K_I, or the J-integral value J_I, which are measures of the stress magnitude at the crack tip. These values are then compared to K_{IC} or J_{IC} to determine the available margin against unstable crack growth. However, the process is defined only for simple structures with simple crack geometry and loading. A vast amount of literature has appeared since 1948 dealing with methods to calculate K_I. The J-integral approach [4] offers a more general and direct method for calculating the stress intensity factor. The method allows the explicit modeling of the crack in a finite element code and the direct calculation of the J-integral, which is a path-independent integral of the strain energy release rate over an arbitrary domain containing the crack. Providing that LEFM conditions apply, equivalence between J_{IC} and K_{IC} (or J_I and K_I) is given by:

$$J_{IC} = \left(1 - \upsilon^2\right) K_{IC}^2 / E \quad \text{for plane strain;} \quad J_{IC} = K_{IC}^2 / E \quad \text{for plane stress;} \tag{1}$$

where υ and E are Poisson's ratio and elastic modulus, respectively. As noted, this relation is valid only when LEFM conditions prevail. However, it is often applied indiscriminately to derive K_{IC} values from J_{IC} tests, sometimes without verifying its applicability. The K_{IC} derived in this manner is referred to as the apparent K_{IC}, or K_{JC}.

The major difference between the K_{IC} and the J_{IC} criteria is that K_{IC} is strictly valid for the condition of small-scale yielding at the crack tip, whereas J_{IC} permits the development of plastic fracture. It is important to point out, however, that the application of the J-integral methodology to plastic fracture can be theoretically justified by making the non-physical assumption that the material behaves as a non-linear elastic material with both loading and unloading occurring along the non-linear stress-strain curve. This assumption is at variance with the true (elastic-plastic) material behavior, and it is acceptable only at crack initiation while the crack tip is in the loading regime. The assumption ceases to be strictly valid during crack extension because the material behind the new crack tip begins to unload elastically as soon as the crack begins to advance. This apparent theoretical limitation on the J-integral has been overlooked in favor of the method's advantages, and the application of the J-integral to elastic-plastic fracture has become the accepted method. Based on this approach, ASTM standards -E399 [5] and -E813 [6] have been developed for determining K_{IC} and J_{IC}, respectively,.

ASTM-valid fracture toughness data quoted in the literature for zirconium alloys, and applied to fuel cladding by inference, were developed from either flat-plate or pressure-tube specimens. Besides obvious geometric differences, such as diameter and wall thickness, from fuel cladding, these specimens have dissimilar material and microstructural characteristics, both in the as-manufactured state and in the service-induced condition.

The primary reason for the absence of direct fracture toughness measurements of cladding geometries is the fact that the ASTM standards restrict the test specimen geometry to limits that cannot be met for the cladding tubes. For example, in order to satisfy the plane-strain-condition requirements for K_{IC} determination, ASTM-E399 restricts the specimen thickness to:

$$B \geq 2.5\left(K_{IC}/\sigma_y\right)^2, \tag{2}$$

where B is the specimen thickness (m), σ_y is the uniaxial yield stress (MPa), and K_{IC} is the fracture toughness (MPa$\sqrt{m}$). Substituting, in the above expression, typical values of σ_y and K_{IC} for irradiated Zircaloy with typical hydrogen content (<500 ppm) gives, at reactor temperatures, values for B of roughly 6 mm, which is 8 to 10 times thicker than typical cladding thicknesses.

For the J_{IC} test, the specimen thickness B and ligament size b (the remaining distance ahead of the crack tip) are limited to:

$$b, B \geq 25 J_{IC}/\sigma_y \tag{3}$$

Because the J-integral is primarily a measure of elastic-plastic (ductile) fracture, J_{IC} in plane-stress specimens is determined from the J-Resistance (J-R) curve by linear regression analysis of J-versus-crack extension measurements obtained from either multiple-specimen tests, or elastic-compliance single-specimen tests. In either test technique, the ligament size must be sufficiently large to allow the development of stable crack growth described by the J-R curve. Unfortunately, this condition cannot be met in cladding fracture tests for radial through-thickness crack orientation, which is the type of crack that can threaten the leak tightness of the fuel rod.

The ASTM thickness restrictions discussed above apply to specimens with circumferential-longitudinal (C-L) crack orientation, i.e., a through-wall crack extending axially under circumferential load. However, the failure mode that is of concern for the retention of fission products is the circumferential-radial (C-R) crack orientation, which is the precursor for the C-L crack. The longitudinal-radial (L-R) crack, which is a guillotine-type fracture, is another failure mode that may threaten the leak tightness integrity of the fuel rod. The appropriate specimen configurations are the arc-shaped specimen for the C-R crack and the bend specimen for the L-R crack. The ASTM criterion that governs the specimen size for both the C-R and L-R cracks is primarily the ligament size, which is the cladding thickness. While it may be possible to create, through cold work and irradiation, a C-L ASTM-valid test specimen with similar texture and irradiation hardness to that of the cladding, doing so for the C-R and L-R fracture orientation is virtually impossible. This is because of the hydride-induced radial variation of fracture properties, as well as the limitation on the development of a J-R curve. Therefore, we are left with only one fracture orientation for which the development of acceptable J_{IC} data is possible,

namely the C-L crack, making the necessary, and generally non-valid, assumption that J_{IC} is the same for all fracture orientations.

Generalizing the fracture toughness measure of J_{IC} developed for the C-L crack orientation to all other crack orientations implies that the cladding microstructure and the hydride morphology created by irradiation and corrosion are homogeneous, which is not the case in general. However, there is evidence to indicate that the error involved may be acceptable for irradiated material *with moderate amounts* of hydrogen concentrations. The effect of irradiation is to eliminate, or greatly reduce, the anisotropy in the material due to changes in *the slip system within the crystallographic texture.*

With respect to the effects of hydrogen, the situation is governed by how hydrogen was introduced in the material and by the amount and orientation of the hydride platelets. For example, hydrogen charging of test samples has homogeneous distribution and orientation of the hydrides, and produces a similar effect to that of irradiation hardening on the fracture toughness. On the other hand, corrosion hydride platelets, when formed in the absence of hoop stress, are oriented preferentially in the circumferential direction because of the initial crystallographic texture. In this orientation, the effect of hydrides on fracture toughness is nearly the same for radially or axially propagating C-R and C-L cracks. Radial hydrides, however, are highly damaging for C-R crack orientation, and their presence can be life-limiting both in-reactor and in storage.

Because of differences in the effects of hydride morphology on fracture toughness, one should keep in mind the source of hydrogen in evaluating the data. Radial hydrides develop when two conditions exist simultaneously: firstly, the solubility limit begins to drop below the local hydrogen concentration as a result of a drop in temperature, and, secondly, when the hydride precipitation occurs in the presence of significant tensile hoop stress. It is not difficult to think of situations where these conditions can coexist during both power operation and spent fuel storage. Because the hydride concentrations vary radially, with the heaviest concentration at the outer surface, the material toughness can vary through the thickness. The overall effect produces crack initiation by brittle fracture, transitioning to ductile fracture in the portion with lower hydrogen concentration, making it difficult to judge the true capacity of the cladding.

3

FRACTURE TOUGHNESS DATA SUMMARY

The data evaluated in the present study spans the period from 1972 to 1996, and is presented in detail in the Appendix. A summary description of the data is presented below.

The data is placed into the following three groups: ASTM-Qualified Fracture Toughness (K_{IC}) Data for Zircaloy-2 (Zr-2) and zirconium with 2.5% niobium (Zr-2.5Nb) Pressure Tubes; ASTM-Qualified Fracture Toughness (K_{IC}) Data for Zircaloy-4 (Zr-4) and Zr-2 Plates; and Non-ASTM J_{IC} Data. Delayed Hydride Cracking data is discussed separately in Section 6

The Zr-2 and Zr-2.5Nb pressure-tube data in the first group, [7 to 12], covers a wide range of conditions, with irradiation levels ranging from zero to 6.5×10^{21} n/cm^2 (E >1 MeV), temperatures from room to 315°C, charged-hydrogen concentrations from as-received to 430 ppm. The most important feature of this group that is of interest to spent fuel is the ductile-brittle transition behavior exhibited by the data. The combined effects of irradiation and changes in hydride orientation modify the brittle-ductile transition behavior. Unirradiated material, with relatively low hydrogen concentration (<100 ppm), exhibits abrupt brittle-ductile transition in the temperature range of 240°C to 280°C, as the hydride orientation becomes co-directional with the applied stress. However, irradiated material exhibits a more gradual transition with temperature. For 200-ppm hydrogen concentration, the lower-shelf K_{IC} values fall in the range of 20 MPa$\sqrt{m}$ to 50 MPa$\sqrt{m}$, and transition gradually to ductile toughness of 80 MPa$\sqrt{m}$ at 280°C. Doubling the hydrogen concentration (to 430 ppm) shifts the upper shelf to 300°C.

The second group consists of two sets of data. The first set [13,14] deals with unirradiated and irradiated Zr-4 plates, with test temperatures in the range of -168°C to 568°C, hydrogen content (as received and charged) from 10 ppm to 250 ppm, and irradiation levels from 0 to 2×10^{21} n/cm^2 (E>1 MeV). The effect of texture on fracture toughness is much stronger for unirradiated material, with variations of a factor of 2. Similar differences are observed between low (<100°C) and reactor operating temperatures. The range of the data, which reflects the effects of temperature, irradiation, texture and hydrogen, is 15 MPa$\sqrt{m}$ to 75 MPa$\sqrt{m}$. The second set [15] in this group includes data for beta-treated Zr-4 and alpha-annealed Zr-2 plate materials and covers a wide range of fluence (0 to 8×10^{21} n/cm^2, E>1 MeV), temperature (20°C to 280°C), and hydrogen concentration (10 ppm to 4000 ppm). Despite the differences in the microstructure from the first material set, the fracture toughness values are similar for similar range of conditions. At room temperature, the values of K_{IC} vary from 20 MPa$\sqrt{m}$ for 500-ppm to 40 MPa$\sqrt{m}$ for 50-ppm hydrogen concentrations. At 280°C the corresponding values of K_{IC} are 30 MPa$\sqrt{m}$ and 60 MPa$\sqrt{m}$, respectively. Higher hydrogen concentrations drive K_{IC} to lower values, approaching 10 MPa$\sqrt{m}$ at 4000 ppm, which far exceeds the hydrogen content of discharged fuel.

The third group of data [16] consists of a single source, and is singled out because it is the only data that deals with cladding geometry. The reported J_{IC} values for unirradiated Zr-2 cladding are of the order of 100 KJ/m^2 at 300°C, which is equivalent to a K_{JC} value of 96 MPa$\sqrt{m}$. This is roughly 50% higher than the plane strain K_{IC}, but it is consistent with ductile fracture.

4

K$_{IC}$ ESTIMATES FOR APPLICATION TO SPENT FUEL

The data for irradiated Zircaloy-2 (Zr-2) and Zircaloy-4 (Zr-4) materials shows the lowest room-temperature K$_{IC}$ values to be in the range of 12 MPa$\sqrt{m}$ to 15 MPa$\sqrt{m}$ for hydrogen concentrations of the order of 1000 ppm. Such low values, however, are typical of beta-quenched material (Ref 15), which has different microstructural characteristics than fuel cladding. A more typical lower-bound value of K$_{IC}$ for end-of-life burnup at 20°C with relatively high hydrogen concentration (~750 ppm) is in the range of 18-20 MPa$\sqrt{m}$. The corresponding K$_{IC}$ value for temperatures above 280°C is 30 MPa$\sqrt{m}$. These K$_{IC}$ values are to be contrasted with 50 MPa$\sqrt{m}$ and higher for moderately irradiated materials with low hydrogen concentrations. The fracture toughness data reviewed in the foregoing supports the following conservative criteria, recommended herein for application to normally discharged fuel with prototypical burnup and hydrogen contents.

$$
\begin{aligned}
&\text{(a)} \quad K_{IC} = 18\,\text{MPa}\sqrt{m} \text{ for } T < 100°C, \ 100 < H < 500\,\text{ppm} \\
&\text{(b)} \quad K_{IC} = 50\,\text{MPa}\sqrt{m} \text{ for } T > 280°C, \ H < 100\,\text{ppm} \\
&\text{(c)} \quad K_{IC} = 30\,\text{MPa}\sqrt{m} \text{ for } T > 280°C, \ 100 < H < 500\,\text{ppm} \\
&\text{(d)} \quad K_{IC} = 20\,\text{MPa}\sqrt{m} \text{ for } T > 280°C, \ 500 < H < 750\,\text{ppm} \\
&\text{(e)} \quad \text{Linear interpolation/extrapolation for } T < 280°C, \ H < 1000\,\text{ppm} \\
&\text{(f)} \quad K_{IC} = 12\,\text{MPa}\sqrt{m} \text{ for any temperature, } H > 1000\,\text{ppm}.
\end{aligned}
\tag{4}
$$

Clearly, the above estimates should not be treated as precise limits. The application of the above criteria in accident analysis is beyond the scope of this report. However, from the user's perspective, it may be instructive to give some guidance and a brief outline of the situations to which the criteria may be applied.

The adoption of fracture-toughness-based evaluation criteria requires the explicit modeling of pre-existing cracks and the calculation of stress-intensity factors. This requires special analysis capabilities and a reliable method of characterizing pre-existing cracks. It will be conservatively assumed that initial flaws and PCI-induced, part-wall cracks may be present in fuel rods at the end of life. The depth of such cracks can vary statistically from an initial, as-manufactured size of 50 microns to a size that depends on service conditions and reactor type (BWR vs. PWR). An earlier study [17] shows that part-wall cracks that are deeper than 40% of the cladding thickness generally require only small power changes to become through-wall cracks. This means that cracks deeper than 40% would have already become part of PCI failure statistics. Therefore, it can be conservatively assumed that the maximum part-wall crack size that can be found in normally discharged fuel placed in storage casks is less than 40% of the cladding thickness.

PCI cracks are C-L type cracks, i.e., oriented radially and axially in the R-Z plane, and can extend only by tensile hoop stress which can be produced by either internal over-pressure or

ovalization deformations resulting from horizontal drop or tip-over. The only other failure mode of interest is the initiation and extension of partial L-R type cracks, which can extend radially and circumferentially under a longitudinal load or axial bending. This failure mode can potentially occur during a horizontal drop or rod buckling during a vertical drop. Unlike the PCI-induced cracks, the L-R crack initiates from an outer-surface defect beneath the oxide layer, and, therefore, the initial crack size cannot be easily estimated. Although there is a tendency to use the outer-surface oxide layer thickness as the initial crack size, it is incorrect to do so because the oxide layer cannot provide the strength and stiffness needed to maintain the required singularity at the crack tip. This places the problem in the regime of crack initiation for which a ductility criterion is needed. Once the crack is initiated in this manner, the analysis method adopted should have the required capability to determine crack extension using the applicable fracture toughness criterion from the above. A detailed description of the possible failure modes experienced by fuel rods during drop accidents is given in Reference 17.

5

FRACTURE-TOUGHNESS CORRELATION

The fracture toughness estimates presented earlier in this report, are derived from data that were not generated for cladding-specific geometry or material conditions. Until such time as ASTM-qualified fracture toughness tests are developed for cladding geometry, fracture toughness estimates applicable to dry storage will continue to be sought. There is great incentive, therefore, to develop an approximation to fracture toughness using easily measurable material properties that reflect actual material conditions and cladding geometry. The intended approximation is a simple correlation that relates the fracture toughness to the critical strain energy density, and is validated by data. As will be shown below, the correlation is derived from fundamental relations of Linear Elastic Fracture Mechanics (LEFM), and is made plausible using physical interpretation of true material behavior.

The critical strain energy density is defined from material property tests as the integral of the product of stresses and strains as follows:

$$U_c = \int_0^{\varepsilon_f} \sigma_{ij} \, d\varepsilon_{ij} \tag{5}$$

In the uniaxial test, the above expression represents the area under the stress-strain curve. Now consider a crack in a plate under a nominal stress σ_N. In such a planar crack, the local stress σ normal to the crack plane at a position ρ ahead of the crack tip can be expressed as:

$$\sigma = K_I / \sqrt{2\pi\rho}, \tag{6}$$

where K_I is the stress intensity factor. It should be noted that by virtue of the singularity at the crack tip, the stress σ is defined everywhere except at the crack tip. Away from the crack tip, the local stress tends to approach the applied far field stress σ_N as shown schematically in Figure-1. It should be noted that Eq. (6) is the consequence of a linear elastic solution of a problem with a stress singularity. This means that although the local stress at some position in the vicinity of the crack tip rises above the yield stress, the stress profile described by Eq. (6) does not recognize the state of plasticity in the material. Such a state would exist within a small region surrounding the crack tip, which is generally referred to as the plastic zone, or the damage zone in brittle materials such as glass and concrete. Although no plasticity is considered in constructing the above expression, it is generally assumed that the solution remains valid outside the plastic zone, including the plastic zone boundary, as schematically shown in Figure 1. A basic assumption made in LEFM is that crack instability occurs when the local stress σ equals the yield stress σ_y [18], where σ_y is the yield stress at the position ρ_y, which leads to the following conditions:

$$\sigma \rightarrow \sigma_y \; , \rho \rightarrow \rho_y \; , K_I \rightarrow K_{IC}$$

Equation (6) can then be rewritten as follows:

$$K_{IC} = \sigma_y \sqrt{2\pi\rho_y} \tag{7}$$

Now we introduce the first of two postulates, namely, to assume instead that the point of instability occurs, not when $\sigma = \sigma_y$, but rather when the elastic strain energy density associated with the LEFM singularity solution reaches the critical value U_c in the neighborhood of the crack tip. As is usual in fracture mechanics, justification for this alternative assumption must come from data. (Note that for elastic-perfectly-plastic material, the above two instability assumptions are equivalent, because for such material the failure condition is only a function of stress regardless of the magnitude of the strain, whereas for strain hardening materials, the stress is not sufficient by itself to describe a limiting condition). Equating the critical strain energy density of the LEFM material to the critical strain energy density of the actual material, we obtain:

$$U_c = \sigma^2/(2E) = \sigma_y \varepsilon_{TE} - \sigma_y \varepsilon_y/2, \tag{8}$$

where σ_y, E, ε_{TE}, ε_y are, respectively, the yield stress, the elastic modulus, the total elongation (elastic + plastic), and the yield strain. The left-hand side of Eq. (8) reflects the presence of crack-tip singularity and the resulting pseudo-elastic stress σ, whereas the right-hand side describes material with distributed damage reflected in the total elongation and the other measured properties. Substituting the quantity $r = \varepsilon_{TE}/\varepsilon_y$, which is a measure of the material's ductility in Eq. (8), we obtain:

$$\sigma_y^2 = 2EU_c/(2r-1) \tag{9}$$

Substituting Eq. (9) in Eq. (6) gives:

$$K_{IC}^2 = 4\pi EU_c \rho_y/(2r-1) \tag{10}$$

For a highly confined crack tip, which is the plane-strain condition imposed on fracture toughness testing, ρ_y is of the order of 10 microns. However, under plane-stress condition, and under conditions of ductile fracture, ρ_y can be an order of magnitude larger. The parameters ρ_y and r play the same physical role in characterizing the level of ductility of the material, and they both increase proportionately with increasing ductility. This suggests a second postulate, namely, that the changes in ρ_y and r occur in such a way that the quantity

$$\rho_y/(2r-1) = 10\times10^{-6} \tag{11}$$

plays the role of a material constant. For example, at an r-value of unity, indicative of totally brittle material, ρ_y has the minimum value of 10 microns, whereas for ductile fracture where r can grow to a value of 10 or greater, the plastic zone size can be of the order of 150-200 microns. Rolfe and Barsum [18] estimated ρ_y to be about 50 times smaller than the plane-strain specimen

thickness B defined in Eq. (2). Using a K_{IC} estimate of 20 MPa$\sqrt{m}$ presented earlier for cladding with relatively high hydrogen content, and 700 MPa as a typical high-burnup yield strength, we calculate an estimate of 40 μm for ρ_y. This gives $r = 2.5$ as the ductility ratio and a total elongation (elastic + plastic) of about 1.8%, which is in the conservative range of the data for high burnup cladding with relatively high hydrogen content. Upon substituting $\rho_y = 10 \times 10^{-6}$ m in eq. (10), we obtain the following simple correlation:

$$K_{IC} = 0.01121\sqrt{E}(U_c)^{1/2} \tag{12}$$

Substituting a typical high burnup value for E of 96,000 MPa in Eq. (12), we obtain:

$$K_{IC} = 3.5\sqrt{U_c} \tag{13}$$

as an approximate upper bound for highly irradiated Zircaloy. In application, the appropriate value of E should be used if available. Otherwise, Eq. (13) is recommended. Comparison of Eqs. (12) and (13) to data for aluminum alloys is shown in Figure 2, which shows excellent agreement. Clearly, there are much more data that can be added to Figure 2.

As discussed in detail above, expressions (12) and (13) make use of two physically-based postulates. The first, which is expressed in Eq. (6), led to the development of Eq. (10). The second postulate, expression (11), is somewhat intuitive, but has its basis in the fact that crack tip local behavior is not independent of the materials macro-mechanical ductility. Both of these postulates lead to a semi-empirical correlation that can be validated by data, and in this sense, they are consistent with the general premise of the Fracture Mechanics Field that is largely empirical. The simplicity of this correlation should not detract from its acceptance, unless it can be shown that it statistically disagrees with fracture toughness data developed in the traditional way. Potential users of this correlation are encouraged to present supporting or counter examples before they adopt or reject its use.

It should be emphasized that the fracture toughness correlation presented above is not intended to replace an ASTM-qualified fracture toughness test for cladding tubes under typical high-burnup conditions. Since such ASTM-qualified tests have not yet been developed, and in view of impending dry storage decisions, the above fracture toughness correlation offers an acceptable alternative. The application of the developed correlation will lead to a conservative assessment of the safety margin, or lack thereof, against cladding rupture in dry storage. As the above-described development would show, this correlation is no more empirical and no less reliable than fracture-toughness-based criteria in other safety-related industries such as the aircraft and pressure vessel industries.
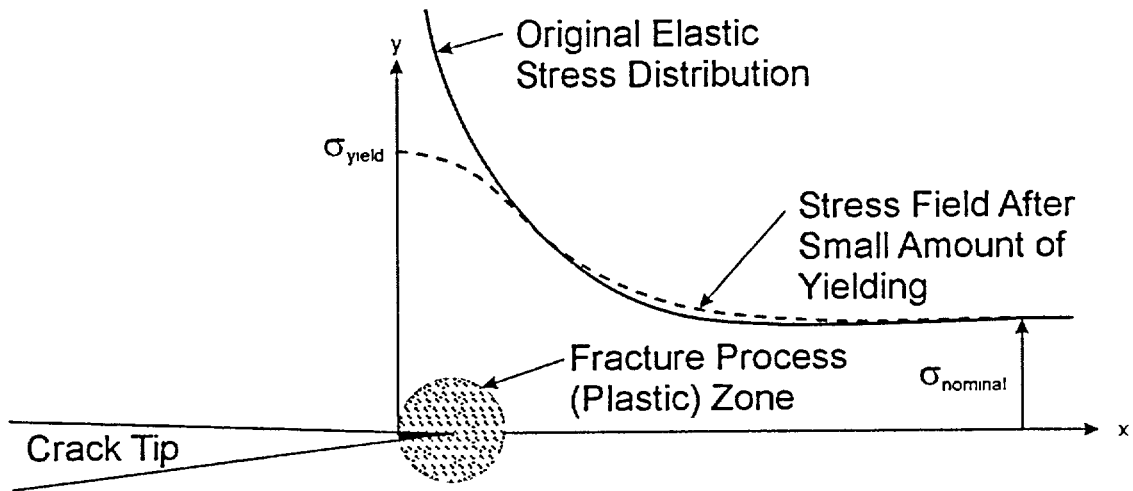
Figure 5-1. Schematic Showing Small Effect of Yielding on Nominal Stress (Ref. 18)
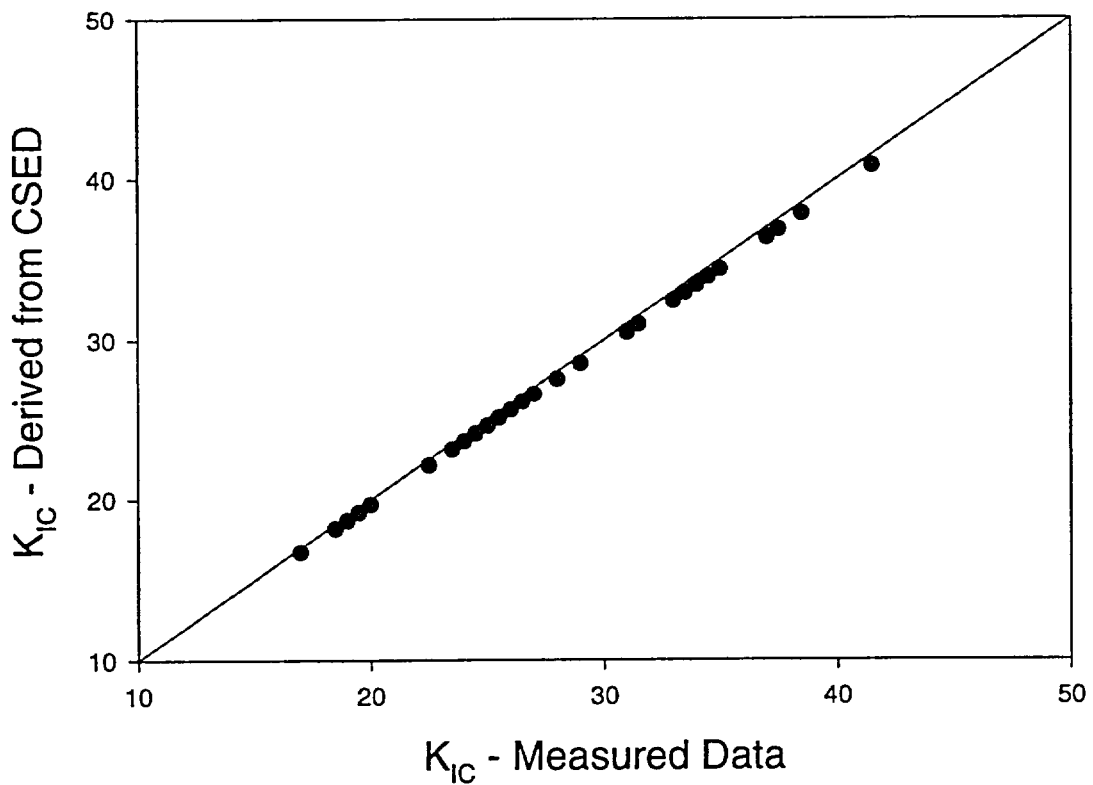
Figure 5-2. Experimental K_{IC} (Ref. 19) vs. K_{IC} Derived from the
Critical Strain Energy Density for Aluminum Alloys

6

DELAYED HYDRIDE CRACKING (DHC)

Delayed hydride cracking (DHC) was first observed to be the responsible mechanism for the cracking and leakage of zirconium with 2.5% niobium (Zr-2.5 Nb) pressure tubes in the CANDU system. As a result, extensive fracture mechanics investigations were undertaken to study DHC in Zr-2 and Zr-2.5 Nb pressure tube materials [19,20]. This section gives a summary description of the DHC phenomenon and discusses its applicability to LWR fuel cladding.

The DHC process evolves in two stages. In the first stage, the process is initiated at a threshold stress intensity factor of the order of 5-6 MPa$\sqrt{m}$. In this threshold regime, the crack velocity increases rapidly with K_I until it transitions into the second stage, which is the stable crack growth stage. The second stage proceeds at a crack velocity that is insensitive to the stress, but it requires a minimum value of stress, characterized by a K_I value in the range 9-10 MPa$\sqrt{m}$, to be sustained. The first stage was found to be independent of temperature; however, the second stage depends on the direction of approach to temperature as will be discussed below. The crack growth rate in the second stage, which determines the failure time under DHC, is governed by the local diffusion rate of hydrogen to the crack tip, with apparent activation energy of about 65 KJ/mol. This is to be compared to the theoretical activation energy of 69.5 KJ/mol for diffusion of hydrogen. The overall process can be summarized as follows:

(1) In the laboratory, the DHC process was found to depend on the direction of approach to test temperature, i.e., whether the test temperature was approached from above or from below. A critical temperature, termed T_{DAT} (Direction of Approach to Temperature), was found such that at a test temperature above T_{DAT}, DHC occurred only when the test specimen was subjected to an over–temperature excursion before testing. Below T_{DAT}, DHC occurred always regardless of whether the material was heated or cooled to the test temperature. However, the crack velocity differs significantly above and below T_{DAT}, depending upon the direction of approach to the test temperature. Below T_{DAT}, the crack growth rate follows an Arrhenius relationship with temperature in either direction; whereas above T_{DAT} the crack velocity decreases rapidly with increasing temperature, but maintains the Arrhenius rate on cooldown. T_{DAT} was found to be about 453K for Zr-2.5 Nb and 423K for Zr-2 materials [20].

(2) Stage-I DHC is initiated at a pre-existing flaw or PCMI-induced part-wall crack, and progresses rapidly to Stage-II.

(3) At constant temperature, the crack velocity during Stage-II is governed by the hydrogen diffusion rate and subsequent precipitation as zirconium hydride at the crack tip, a process that is driven by the stress gradient created by the crack. The hydrogen diffusion is enhanced under temperature cycling as discussed in (1) above.

(4)   As the hydride precipitation continues, the crack tip hydride eventually grows to a critical size upon which it fractures, allowing the crack to extend a short distance equal to the size of the hydride, and is arrested in the tougher material.

(5)   The newly formed crack tip re-initiates the process of hydrogen diffusion and precipitation described in Steps (3) and (4). The crack continues to extend in this intermittent manner until cladding fracture is completed by plastic instability.

For the DHC process to become operative in spent fuel storage, the following conditions must exist:

(1)   Presence of cracks at the inside diameter.

(2)   A crack-tip confinement such that a tri-axial tensile stress state exist to facilitate the diffusion of hydrogen into the crack process zone and subsequent precipitation of hydrides.

(3)   Sufficient hydrogen concentration.

(4)   Storage temperature below T_{DAT} (423K), or temperature cycling above T_{DAT}.

(5)   Stress intensity factor of 10 MPa$\sqrt{m}$ or higher.

Condition (1) is satisfied. The presence of flaws and PCI-induced, part-wall cracks are unavoidable in discharged fuel. However, as argued earlier, no part-wall cracks greater than 40% of cladding thickness can exist in non-failed fuel rods at the end of life, but such cracks remain sub-critical with respect to Stage-I DHC under typical storage stresses.

Condition (2) would depend on the geometry. In thick pressure tubes and test plate specimens, the thickness is such that plane-strain conditions exist. Consequently, a state of tri-axial tension can develop, which clearly prevailed in the DHC tests reported in the literature. In LWR cladding, however, plane-stress condition dominates and a condition of biaxiality rather than triaxiality would exist, which is a weaker form of crack-tip confinement. This would lead us to conclude that hydride formation at the crack tip process zone would require a higher stress field than in plane-strain states. Precise quantification of this effect requires experimental verification, and until then, we have to assume, conservatively, that Condition (2) is also satisfied.

Condition (3) is easily satisfied. Although the crack velocity during Stage-II of the DHC process can depend on the hydrogen concentration, this dependence is not strong and DHC cracking can occur at very low hydrogen concentrations.

Condition (4) is partially satisfied, in the sense that, once the fuel is placed in dry storage, thermal cycling during dry storage is not expected to occur and, consequently, the acceleration of the DHC process by thermal cycling above T_{DAT} is not relevant. However, the fuel will continue to be under decaying temperature, and will eventually be at temperatures below T_{DAT}.

Condition (5) is the dominant factor in the sense that DHC cannot exist without sufficient stress even if all other conditions are satisfied. It requires calculations to determine if the stress intensity factor due to fission gas pressure can rise to the threshold value. We first consider a BWR (Zr-2) rod under an internal gas pressure of 7.5 MPa, which is the maximum it can be at the reactor operating temperature of 560K. At a T_{DAT} of 423K, the rod pressure is 5.65 MPa. Considering a maximum possible crack size of nearly half the cladding thickness, as discussed above, we calculate a stress intensity factor of about 2 MPa$\sqrt{m}$, which is well below the threshold value for Stage-I, and is a factor of 5 smaller than Stage-II fracture toughness. For a PWR rod under the same assumptions, namely, rod pressure equal to reactor system pressure at reactor temperature, K_I for 40% crack is calculated to be less that 5 MPa$\sqrt{m}$, which even if initiated is a factor of 2 smaller than Stage-II fracture toughness.

Therefore, it can be concluded on the basis of the above argument that DHC is not an operative mechanism for LWR fuel rods in storage.

7

REFERENCES

1. *U.S. Code of Federal Regulations*, "Licensing Requirements for the Independent Storage of Spent Nuclear Fuel and High-Level Radioactive Waste," Part 72, Title 10, "Energy".

2. U.S. Nuclear Regulatory Commission, "Standard Review Plan for Dry Cask Storage System: Final Report," NUREG-1536, January 1997.

3. U.S. Nuclear Regulatory Commission, "Standard Review Plan for Spent Fuel Transportation," NUREG-1567, January 1997.

4. Rice, J.R., "A Path Independent Integral and the Approximate Analysis of Strain Concentration by Notches and Cracks," Journal of Applied Mechanics, Transactions ASME, 35, June 1968.

5. ASTM-E399, "Standard Test Method for Plane-Strain Fracture Toughness of Metallic Materials," *1989 Annual Book of ASTM Standards*, Vol. 3.01.

6. ASTM-E813-88, "Standard Test Method for J_{IC}, A Measure of Fracture Toughness," *1989 Annual Book of ASTM Standards*, Vol. 3.01.

7. Barsell, A.W., "Nonlinear Statistical Analysis of Zircaloy-2 Fracture Toughness Data," Internal Correspondence, GA Technologies, San Diego CA, February 1987.

8. Davies, P.H. and Stearns, C.P., "Fracture Toughness Testing of Zircaloy-2 Pressure Tube Material with Radial Hydrides Using Direct-Current Potential Drop," ASTM STP 905, 1986, pp. 379-400.

9. Coleman, C.E., Cheadle, B.A., Causey, A.R., Chow, P.E.K., Davies, P.H., McManus, M.D., Rodgers, D.K., Sagat, S. and van Drunen, G., "Evaluation of Zircaloy-2 Pressure Tubes from NPD," ASTM STP 1023, 1989, pp. 35-49.

10. Wallace, A.C., Gordon, K.S., and Lepik, O.E., "Effects of Hydride Morphology on Zr-2.5 Nb Fracture Toughness," ASTM STP 1023, 1989, pp. 66-88.

11. Huang, F.H. and Mills, W.J., "Fracture and Tensile Properties of Irradiated Zircaloy-2 Pressure Tubes," Nuclear Technology 102, 3, 1993, p. 367.

12. Huang, F.H., "Brittle-Fracture Potential of Irradiated Zircaloy-2 Pressure Tubes," Journal of Nuclear Materials 207, 1993, p. 103.

13. Walker, T.J., "Characterization of the Fracture Toughness of Zircaloy," Nuclear Technology, Vol. 16, 1972, p. 509.

14. Walker, T.J. and Kass, J.N., "Variation of Zircaloy Fracture Toughness in Irradiation," ASTM STP 551, 1974, pp. 328-354.

15. Kreyns, P.H., Bourgeois, W.F., White, C.J., Charpentier, P.L., Kammenzind, B.F., Franklin, D.G., "Embrittlement of Reactor Core Materials," Zirconium in the Nuclear Industry: 11th International Symposium, ASTM STP 1295, American Society for Testing and Materials, 1996, pp. 758-782.

16. Grigoriev, V., Josefsson, B., and Rosborg, B., "Fracture Toughness of Zircaloy Cladding," ASTM STP 1295, 1996, pp. 435-447.

17. Sanders, T.L., et al., "A Method for Determining the Spent-Fuel Contribution to Transport Cask Containment Requirements," Sandia Report SAND90-2406, TTC-1019, UC-820, November 1992.

18. Rolfe, S.T. and Barsom, J.M., *Fracture and Fatigue Control in Structures, Application of Fracture Mechanics*, Prentice-Hall, Inc., Englewood Cliffs NJ.

19. *Proceedings of an International Symposium on Absorbed Specific Energy and/or Strain Energy Density Criterion*, Sept. 17-19, 1980, G.C. Sih, E. Czoboly, F. Gillemot, Editors, Martinus Nijhoff Publishers, The Hague/Boston/London.

20. Huang, F. H. and Mills, W. J., Delayed Hydride Cracking Behavior for Zircaloy-2 Tubing," Metallurgical Trans. A, 22A, P. 2049, 1991.

APPENDIX A: FRACTURE TOUGHNESS DATA

The data discussed in the report is extracted from the cited sources and is presented in this appendix to provide the user with easy access in a single source. The data is grouped into the following three groups:

(1) ASTM-Qualified Fracture Toughness (K_{IC}) Data for Zr-2 and Zr-2.5 Nb Pressure Tubes

(2) ASTM-Qualified Fracture Toughness (K_{IC}) Data for Zr-4 and Zr-2 Plates

(3) Non-ASTM J_{IC} Data

Group I: Zr-2 and Zr-2.5 Nb Pressure Tubes and Plates

Barsell [Ref. 7]: This 1987 data was generated for N-reactor pressure-tube Zr-2 material as function of temperature and fluence. The fluence varies from 0.2×10^{21} to 6.5×10^{21} n/cm² (E>1 MeV). The test temperature varies from room temperature to 600°F, with the majority of the data below 400°F. Barsell developed the following correlation for the data:

$$K_{IC} = Exp\left(A - 0.14\phi + 2.3 \times 10^{-4} T\phi\right)$$

where

$$A = 3.73 + 5 \times 10^{-4} T \quad \text{for axial cracks}$$
$$A = 3.81 + 2 \times 10^{-4} T \quad \text{for circumferential cracks}$$

Units:

ksi$\sqrt{in}$	for K_{IC}
°F	for T
10^{21} n/cm²	for ϕ (E > 1 MeV)

The K_{IC} values in this data varied from 17.5 ksi$\sqrt{in}$ to 68.6 ksi$\sqrt{in}$ (19.25 MPa$\sqrt{m}$ to 75.5 MPa$\sqrt{m}$) with standard deviation of about 5 ksi$\sqrt{in}$ (5.5 MPa$\sqrt{m}$). This data is used extensively because of the convenient way it is presented and its ready availability.

Davies et al., Coleman et al., and Wallace et al. [Refs. 8,9,10]: These papers are grouped together because they deal with a common theme, namely, the effects of hydride morphology on the fracture toughness. Davies' and Wallace's papers deal with unirradiated Zr-2 and Zr-2.5 Nb, and

Coleman's paper deals with irradiated Zr-2; all are pressure tube materials. The test temperatures varied between room temperature and 280°C. The unirradiated material had low hydrogen concentrations (<100 ppm), and charged in the presence of stress to introduce varying hydride orientations. The data indicate a brittle-ductile transition that varied with temperature and hydrogen concentrations. The upper shelf fracture toughness varied over a wide range, from 75 MPa$\sqrt{m}$ to 175 MPa$\sqrt{m}$. The lower shelf fracture toughness varied from 20 MPa$\sqrt{m}$ to 50 MPa$\sqrt{m}$. The combined effect of irradiation and temperature on fracture toughness is to change the brittle-ductile transition behavior. The unirradiated material exhibits abrupt brittle-ductile transition in the temperature range of 240°C to 280°C. However, the irradiated material exhibits more gradual transition with temperature, with complete transition to ductile toughness of 80 MPa$\sqrt{m}$ at 240°C with 200 ppm and at 300°C with 430 ppm.

Huang et al. and Huang [Refs. 11,12]: These two papers deal with the fracture properties of irradiated Zircaloy-2 pressure tubes. The irradiation levels vary from 0 to 6.1×10^{21} n/cm^2 (E>1 MeV). The test temperature is in the range of 32°C to 177°C with few tests conducted at 260°C. Both testing methods were used, namely, ASTM-E399 (K_{IC}) and ASTM-E813 (J_{IC} or K_{JC}). The magnitudes of K_{IC} and K_{JC} vary between 18 MPa$\sqrt{m}$ (32°C, 5.6×10^{21} n/cm^2, E>1 MeV) and 55 MPa$\sqrt{m}$ (177°C, 0.2×10^{21} n/cm^2, E>1 MeV). The K_{JC} values for unirradiated material were 20% to 40% higher.

Group II: Zr-4 Plates

Walker, Walker and Kass [Refs. 13,16]: These papers deal with unirradiated and irradiated Zr-4 plates tested in accordance with ASTM-E399 requirements for plane strain specimens (1"-thick plates). The test temperatures vary from -200°F to 600°F, hydrogen content (as received and charged) from 10 ppm to 250 ppm, and irradiation levels from 0 to 2×10^{21} n/cm^2 (E>1 MeV). The data shows large dependence of the fracture toughness on texture in the unirradiated state, with a minimum to maximum range of 35 ksi$\sqrt{in}$ to 70 ksi$\sqrt{in}$. The irradiated samples show less dependence on texture. An interesting result is the slight increase of fracture toughness with irradiation for room temperatures and higher, which is contradictory to the pressure tube data for Zr-2 and Zr-2.5 Nb. The effect of hydrides is to reduce fracture toughness by a factor of 1.5 to 2 for 250 ppm for temperatures below 200°F, with the largest reduction at -100°F. The data trend, however, shows small effects at higher (reactor operating) temperatures for hydrogen concentrations of the order of 250 ppm. The range of the data, which reflects the effects of temperature, irradiation, texture and hydrogen, is between 15 ksi$\sqrt{in}$ for -100°F, 250 ppm, irradiated material, to 65 ksi$\sqrt{in}$ for non-hydrided non-irradiated material at 300°F.

Kreyns et al. [Ref. 15]: This is one of the more recent papers (1996). It includes data for beta-treated Zr-4 and alpha-annealed Zr-2 plate materials and covers a wide range of fluence (0 to 8×10^{25} n/m^2, E>1 MeV), temperature (20°C to 280°C), and hydrogen concentration (10 ppm to 4000 ppm). Moreover, while the material is reactor grade, the microstructure is not typical of modern cladding materials. The hydrogen was introduced by charging, and therefore, the hydrides differ in morphology from corrosion hydrides. However, the concentrations far exceed those for discharged fuel. At room temperature, the values of K_{IC} vary from 20 MPa$\sqrt{m}$ for 500 ppm hydrogen concentrations to 40 MPa$\sqrt{m}$ for 50 ppm hydrogen concentration. At 280°C the corresponding values of K_{IC} are 30 MPa$\sqrt{m}$ and 60 MPa$\sqrt{m}$, respectively. Higher hydrogen

concentrations drove K_{IC} to lower values, approaching 10 MPa$\sqrt{m}$ at 4000 ppm hydrogen concentration.

Group III: J_{IC} for Zr-2 Cladding Geometry (Non-ASTM)

Grigoriev et al. [Ref. 16]: This is the first example of fracture toughness tests for cladding geometry. The test specimen thickness and ligament size do not satisfy ASTM-E813 requirements for J_{IC} testing. Therefore, the data has to be considered non-valid by ASTM standards. However, in view of the fact that none of the previous fracture tests, while conforming to ASTM requirements, are as representative of cladding geometry as the data in this group, the J_{IC} data should be viewed as worthy of further evaluation. The reported J_{IC} values for unirradiated Zr-2 cladding are of the order of 100 KJ/m^2 at 570K, which is equivalent to a K_{JC} value of 96 MPa$\sqrt{m}$. This is roughly twice the plane strain K_{IC}, but it is consistent with ductile fracture. The Grigoriev paper is the first of an emerging testing literature for which an ASTM standard will become necessary.

Table A-1 (Ref. 9)
COMPUTER DATA LIST FOR AXIAL CRACKS

Temperature (F)	Fluence	K_{IC} (ksi $\sqrt{in}$)
80	1.10	39.7
80	1.20	38.0
90	3.70	28.9
90	5 00	25 8
90	5 00	24.6
90	5.00	23.6
90	4.60	23.2
90	4 60	26.8
212	5.00	32.7
350	3 70	38.2
350	5 00	37.1
350	5.00	39.2
350	4.60	41.5
350	4 60	43.2
350	4.60	32.3
350	4.60	43.9
500	5.00	41.1
90	0.70	38.9
350	0.70	45.9
90	2.40	38.4
350	2.40	42.3
350	2.40	46.3
90	4.10	28.3
350	4.10	38.4
80	0.05	37.2
80	0.05	46.8
80	0.05	38.5
350	0.05	45.4
212	0.05	42.7
80	4.20	20.7
80	4.20	19.6
80	4.20	21.6
350	4.20	39.2
350	4.20	44.2
212	4.20	31.3
212	4.20	25.8
120	4.20	21.6
170	4.20	24.6
250	4.20	35.2
300	4.20	39.2
212	4.20	29.5
80	4.50	19.3
80	4.50	18.1
212	4.50	29.6
350	4.50	37.9
212	4.50	31.0
170	4.50	24.4
80	4.50	19.9
120	4.50	21.7
350	4.50	46.4

Table A-1 (Ref. 9)
COMPUTER DATA LIST FOR AXIAL CRACKS
(Continued)

Temperature (F)	Fluence	K_{IC} (ksi $\sqrt{in}$)
80	3.90	23.4
80	3 90	25 8
212	3 90	35.5
212	3.90	33 8
80	3.90	23.9
350	3.90	53.0
170	3 90	30 4
350	4.20	50.0
500	4 20	61 0
350	0 43	58 5
80	0 00	37.3
80	2 30	34.2
80	2.60	28 9
80	0 80	40 7
80	0 70	46 0
80	3.50	17.5
80	3 50	20 9
350	3.50	44.0
500	3 50	42 0
80	3.50	19.7
80	3.50	19.9
80	1.80	50.1
90	4 90	38.7
90	2.20	33.7
212	4 90	40.5
350	2.20	46.3
350	4.90	42.9
350	4.90	45.3
500	4 90	47.0
446	6.50	36.4
446	6 50	45.8
446	6 50	44.3
446	6.50	48.8
446	6.50	44.1
536	6.50	50.1
536	6.50	51.5
536	6.50	39.1
536	6.50	57.5
536	6.50	63.1
536	6.50	57.5
536	6.50	60.9
536	6.50	59.8
536	6.50	68.6
536	6.50	41.9
536	6.50	56 4
80	6.50	18 0
80	6.50	18.3
80	6.50	22 5
80	6.50	21.7

A-5

Table A-2 (Ref. 9)
COMPUTER DATA LIST FOR CIRCUMFERENTIAL CRACKS

Temperature (F)	Fluence	K_{IC} (ksi $\sqrt{in}$)
80	4.2	23.0
80	4.2	22.8
80	4.2	20 5
212	4.2	26.8
212	4.2	23.2
350	4.2	34.9
350	4.2	37.4
250	4.2	28 8
300	4.2	30 1
90	4.9	33.7
350	4.9	36.1
90	5.0	23 0
350	5.1	33.1
90	5.1	28 5
90	5.1	25 1
350	5.1	26.2
350	5.1	27.4
350	5.1	41.4
90	0.2	41.3
90	0.2	49.0
350	0.2	49.9
350	0.2	46 1
350	0.2	45.3
350	0.2	48.2
90	4.1	33.7
90	4.1	33.5
350	4.1	42.5
350	4.1	41.4
350	4.1	44.5

A-6

Table A-3 (Ref. 10)
SUMMARY OF TEST DATA

Specimen	[H] mg/kg	HCC	Test Temperature (°C)	K_{max} MPa • m$^{1/2}$
Strip 1				
1	62	0	23	80.2
4	-	-	23	94 0
3	-	-	175	132.9
6	-	-	175	140.8
2	-	-	240	132.3
5	-	-	240	133.4
Strip 1A				
1	69	0.27	23	38 6
3	-	0 50	175	46 9
2	-	0.30	240	139.4
Strip 2				
3	83	0 57	175	41.1
2	76	0.55	240	76 2
1	75	0 56	240	141.7
4	75	0.54	240	132.3
Strip 3				
1	69	0 11	23	58.7
3	70	0.11	175	123.3
2	-	0 11	240	144.2
Tube 1				
1	-	0.13	23	60 8
2	-	-	23	61 1
3	-	-	23	59.9
9	49	-	100	112 8
7	-	-	175	111.2
8	54	-	175	133.5
5	-	-	240	118 2
6	-	-	240	109.3
Tube 2				
A1	-	0 04	23	80 4
C1	-	-	23	81.9 '
A2	40	-	100	113.8
C2	44	-	100	106 6
A3	38	-	175	123.7
C3	44	-	175	115.0
B1	33	-	240	110.1
D1	-	-	240	111 1

Table A-4 (Ref. 11)
FRACTURE TOUGHNESS OF IRRADIATED ZIRCALOY-2 PRESSURE TUBES

Crack Orientation	Test Temperature (°C)	Fluence (10^{21} n/cm^2)	Hydrogen (ppm)	K_{IC} (MPa$\sqrt{m}$)	K_C (MPa$\sqrt{m}$)
C-L	32	2.2	<4	37.1	-
C-L	32	4.9	14	39.7	-
C-L	100	4.9	6	-	44.0
L-C	32	4.9	25	37.1	-
C-L	32	0.7	40	-	42.7
C-L	32	2.4	20	-	42.2
C-L	32	3.7	34	31.8	-
C-L	177	3.7	34	-	42 0
C-L	32	4.6	138	25.5	-
C-L	177	4.6	84	-	45.7
C-L, Outer	177	4.6	30	-	47.5
C-L, Inner	177	4.6	259	-	45.6
C-L	32	5.0	89	26.0	-
C-L, Outer	32	5.0	16	27.6	-
C-L, Inner	32	5.0	205	26.5	-
C-L	100	5.0	90	36.0	-
C-L	177	5.0	52	-	40.8
L-C	32	5.0	35	25.3	-
L-C	177	5.0	20	35.1	-
Weld, C-L	32	4.1	35	31.1	-
Weld, C-L	177	4.1	35	-	42.2
Weld, C-L	32	5.1	151	27.4	-
Weld, C-L	177	5.1	92	-	30.1
Weld, C-L	177	5.1	159	28.8	-
Weld, C-L	260	5.1	144	-	45.5
Weld, L-C	32	4.1	35	36.9	-

Table A-5 (Ref. 11)
J_{IC} FRACTURE TOUGHNESS TEST RESULTS BASED ON J-R CURVE REGRESSION ANALYSIS

Crack Orientation	Test Temperature (°C)	Fluence (10^{21} n/cm^2)	Hydrogen (ppm)	K_C (MPa$\sqrt{m}$)	K_{JC} (MPa$\sqrt{m}$)
C-L	177	2.2	<4	50.9	52.4
C-L	177	4.9	<4	49.8	52.9
C-L	177	4.9	6	47.2	49.7
C-L	260	4.9	<4	51.7	50 9
L-C	177	4.9	9	39.7	41.8
C-L	177	0.7	40	50.5	47.3
C-L	177	2.4	20	46.5	40.0
C-L	177	2.4	20	50.9	49.5
C-L	260	5.0	111	45.2	46 6
Weld, L-C	32	0.2	50	-	45 4
Weld, L-C	32	0.2	50	-	53.9
Weld, L-C	177	0 2	50	-	54 9
Weld, L-C	177	0 2	50	-	50 7
Weld, L-C	177	0.2	50	-	49 8
Weld, L-C	260	0 2	50	-	53 0
Weld, L-C	177	4 1	35	46.8	-
Weld, L-C	260	4.1	35	49.0	-

Table A-6 (Ref. 12)
FRACTURE TOUGHNESS OF IRRADIATED ZIRCALOY-2 PRESSURE TUBES

Crack Orientation	Test Temperature (°C)	Fluence (10^{25} n/m^2)	Hydrogen (ppm)	K_{IC} (MPa$\sqrt{m}$)	K_C (MPa$\sqrt{m}$)
C-L	32	3 3	3	-	42.4
C-L	177	3.3	-	-	42.8
C-L	260	3.3	-	-	38.7
C-L	260	3.3	-	-	35.8
C-L	32	5 6	-	20 0	-
C-L	32	5.6	-	18 4	-
C-L	177	5.6	72	29.2	-
C-L	177	5.6	-	30.7	-
C-L	177	5.6	-	26 8	-
C-L	260	5.6	150	29.5	-
C-L	32	6.1	34	31.2	-
C-L	177	6.1	64	31.2	-
C-L	260	6.1	-	-	38.0
C-L	260	6.1	-	-	37.7
C-L	32	4.5	220	21.7	-
C-L	177	4.5	-	26 5	-
C-L	177	4.5	-	26.7	-
C-L	260	4.5	-	-	45.2
C-L	32	2.4	20	-	42.2
C-L	32	5.0	89	26 0	-
C-L	177	5.0	52	-	40.8

Table A-7 (Ref. 12)
J_{IC} FRACTURE TOUGHNESS TEST RESULTS BASED ON J-R CURVE REGRESSION ANALYSIS (Tube 2954)

Crack Orientation	Test Temperature (°C)	Fluence (10^{25} n/m^2)	K_{JC} (MPa$\sqrt{m}$)
C-L	32	0.0	72.8
C-L	177	0.0	68.6
C-L	177	0.0	66 4
C-L	260	0.0	79.5
C-L	260	0.0	74.9
C-L	260	5.6	34.4

Table A-8 (Ref. 13)
ZIRCALOY FRACTURE TOUGHNESS DATA

Specimen Type	Specimen Orientation	Test Temperature (°F)	Failure Load (lb)	Failure K_{JC} [ksi (in)$^{1/2}$]	Secant K_{JC} [ksi (in)$^{1/2}$]
1 X WOL	TW	-150	3475	34 5	-
		-150	3460	35 6	35.5
		-102	3660	38 0	-
		-100	3690	36 0	-
		-52	3830	37.5	37.0
		-2	3600	37.4	-
		+75	3700	41.8	40 3
		+75	4850	52.3	39 6
		+125	6100	58 6	44.2
		+175	5400	58 2	43 5
		-152	3840	34.7	-
		-150	4500	42.0	-
		-150	3750	32 9	-
		0	4640	42 0	-
		-2	4210	39.6	-
0 4 X CT	TW	-150	1325	35 5	-34.8
		-100	1350	36 8	34 9
		-43	1250	36.2	35 1
		-50	1250	37 2	36 6
		0	1510	36 2	34 6
		0	1430	39.2	36 2
		+75	1390	43.4	30.3
		+75	1500	43.4	31.8
		+125	1625	43.1	32.4
		+175	1600	44 7	30 1
0 4 X CT	RT	-98	1325	43 0	36 6
		-102	1380	43.3	34.5
		-2	1290	42.3	31.2
		0	1265	41.9	30 8
0 4 X CT	WT	-100	1320	38.8	38.2
		-100	1100	34.0	33.5
		0	900	37.9	32.0
		+1	1640	45.0	35.6

Table A-8 (Ref. 13)
(Continued)

Specimen Type	Specimen Orientation	Test Temperature (°F)	Failure Load (lb)	Failure K_{IC} [ksi (in)$^{1/2}$]	Secant K_{IC} [ksi (in)$^{1/2}$]
0.4 *X* CT	RW	-100	1790	48.0	41.8
		0	1480	36.6	35.1
		0	1590	38.6	35.2
		+76	2000	47.7	30.6
		+77	2120	51.0	36.1
		-150	1475	44.5	40.7
		+100	1650	40.1	36.0
		+77	2225	53.0	42.9
0.4 *X* CT	TR	-100	1390	52.3	46 4
		0	2200	56.9	42.8
		0	2500	60.0	39 8
		+76	2280	59.7	37.2
		+76	2320	59.5	38 0
		-150	1750	42.1	-
		-100	1890	50.8	46.0
		-100	2080	53.5	46.3
		+100	2320	58 8	42.9
		+76	2270	59.0	40.9
0.4 *X* CT	$\dot{\varepsilon} \propto 0.2$ in/min	+76	2350	52 7	32.6
	$\dot{\varepsilon} \propto 1.0$ in/min	+76	2475	49.2	37.1
	$\dot{\varepsilon} \propto 2.0$ in/min	+76	2145	54.5	38.5

A-11

Table A-9 (Ref. 14)
EFFECT OF IRRADIATION ON FRACTURE TOUGHNESS OF
IRRADIATED ZIRCALOY-4 TEST DATA SUMMARY

Description	Valid	Est. Fluence (nvt × 10²⁰) (n/cm²)	Meas. Fluence (nvt × 10²⁰) (n/cm²)	Test Temperature °F	$K_{IC_{SECANT}}$ psi√in	$K_{IC_{MAX}}$ psi√in
FT-1	Yes	5.6	7	RT	-	45900
Unhydrided	Yes	5.6	7.95	176	43000	55000
α-annealed Zr-	No	5.3	7.66	600	21800	41600
4	No	5.3	7.51	400	31200	48600
Ingot R-59	Yes	4.9	7.17	RT	45600	-
TW	Yes	4.9	7.07	0	23900[C]	23900[C]
Orientation	Yes	5.1		-100	-	34200
	Yes	5.1		25	-	42000
	Yes	15.3		RT	-	50800
	Yes	15.3		200	53500	61000
	Yes	15.1		RT	48500	48500
	Yes	15.1		RT	-	51600
FT-2 Hydrided	Yes	5.1		RT	20100	20100
to	Yes	5.1		175	33400	33400
250 ppm	Yes	9.6	10.35	RT	23000	23000
α-annealed Zr-	Yes	9.6	9.60	-100	16700	16700
4	Yes	13.5		RT	22000	22000
Ingot	Yes	13.5		175	20000[C]	20000[C]
WC377671Q	Yes	20.8		300	31400[D]	31400
TW	Yes	20.8		300	-	-
Orientation	Yes	20.8		450	40700	40700
	Yes	20.8		450	41200	43000
	Yes	20.8		600	42500	42500
	Yes	20.8		600	45400	45400
FT-3 Hydrided	Yes	4.9		RT	26200	26200
to	Yes	4.9		175	26000	26000
250 ppm	Yes	9.2	9 4	175	27800	27800
α-annealed Zr-	Yes	9.2	10 0	RT	25000	25000
4	Yes	12.8		RT	26900	26900
Ingot	Yes	12 8		300	65000	65000
WC377671Q	Yes	20.5		RT	24600	24600
WT	No[E]	20.5		450	43600	47400
Orientation						

Table A-9 (Ref. 14)
(Continued)

Description	Valid	Est. Fluence (nvt × 10^{20}) (n/cm²)	Meas. Fluence (nvt × 10^{20}) (n/cm²)	Test Temperature °F	$K_{IC_{SECANT}}$ psi√in	$K_{IC_{MAX}}$ psi√in
FT-4	Yes	2.4		RT	38200	*B*
Unhydrided	Yes	2.4		0	*B*	*B*
σ-annealed Zr-4	Yes	5.0		0	-	40300
	Yes	5.0		RT	42100	*B*
Ingot	Yes	9.8	9.6	175	46200	59200
WC377671Q	Yes	9.8	10 13	-100	27400	27400
TW	Yes	9.8		-100	*B*	*B*
Orientation	Yes	9.8		RT	-	46500
	Yes	18.9		-100	-	32800
	Yes	18.9		-100	*B*	-
	Yes	19.0		0	-	32500
	Yes	19.0		0	52000[C]	72500[C]
	Yes	19.1		RT	52400	*B*
	Yes	19.1		RT	54500	54500
	Yes	19.0		200	55200	*B*
	Yes	19.0		200	54600	63500
	No	19.0		200	46800	59000
	A	19.0		200[A]	-	58500
FT-5	Yes	9.8		RT		52800
Unhydrided	Yes	9.8		175	48000	55800
σ-annealed Zr-4						
Ingot						
WC377671Q						
WT						
Orientation						
FT-6	Yes	5.2		-100		34600
Unhydrided	Yes	5.2		175	49900	49900
α-annealed Zr-4						
Ingot						
WC377671Q						
RT Orientation						
FT-7	Yes	10 2	10.35	RT		39900
Unhydrided	Yes	10 2	10 9	175	55600	58300
β-quenched Zr-4						
Ingot						
WC377671Q						
WT						
Orientation						

Table A-9 (Ref. 14)
(Continued)

Description	Valid	Est. Fluence (nvt × 10²⁰) (n/cm²)	Meas. Fluence (nvt × 10²⁰) (n/cm²)	Test Temperature °F	$K_{IC_{SECANT}}$ psi√in	$K_{IC_{MAX}}$ psi√in
FT-8 Hydrided	Yes	10.1	10.35	RT	25200	25200
to 250 ppm	Yes	10 1	10.75	175	25600	25600
β-quenched	Yes	20.4		RT	24600	24600
Zr-4 Ingot WC377671Q WT Orientation	No[E]	20.4		500	47700	47700

A   Validity impossible to determine due to strain gage failure.
B   Specimens unloaded rapidly after $K_{IC_{SECANT}}$ for sectioning to allow for plastic zone size determination.
C   Validity highly questionable due to excessively long fatigue crack.
D   Specimen improperly loaded.
E   Thickness required for ASTM valid test ~0.6 in.

Table A-10 (Ref. 14)
SUMMARY OF NON-IRRADIATED ZIRCALOY FRACTURE TOUGHNESS DATA

Orientation	H_2 ppm	Test Temperature °F	$K_{IC_{SECANT}}$ psi√in	$K_{IC_{MAX}}$ psi√in
TW	10	-250	33200	-
	10	-250	36100	-
	10	-150	34400	-
	10	-150	34700	-
	10	-150	42000	-
	10	-150	41500	-
	10	-146	41200	-
	10	-148	41100	-
	10	-151	41600	-
	10	-150	32400	-
	10	-150	36600	-
	10	-150	47500	-
	10	-100	38500	39900
	10	-100	41000	42500
	10	-50	42600	-
	10	-50	40300	-
	10	-50	38800	-
	10	0	39000	-
	10	0	36200	-
	10	0	38500	40700
	10	0	36800	37400
	10	0	36000	-
	10	0	36300	-
	10	0	36500	42000
	10	0	39100	43000
	10	43	-	42500
	10	50	-	42500
	10	100	46500	57200
	10	100	-	42000
	10	100	47000	51300
	10	140	51000	54000
	10	175	51000	51000
WT	10	-150	39400	39400
	10	-50	39300	-
	10	0	43000	47700
	10	0	44700	49200
RT	10	-150	40200	55000
	10	0	38000	43000
	10	0	38200	42100
	10	-50	-	43100
	100	50	-	42000
	10	1000	-	39400

Table A-10 (Ref. 14)
(Continued)

Orientation	H_2 ppm	Test Temperature °F	$K_{IC_{SECANT}}$ psi√in	$K_{IC_{MAX}}$ psi√in
WR	10	-150	56100	65000
	10	-100	-	59600
	10	-100	44900	-
	10	-100	41200	-
	10	0	38300	-
	10	0	36900	-
	10	0	-	62400
	10	100	30500	58500
	10	100	-	58000
TW	250	-100	-	-
	250	0	20100	-
	250	0	19200	20900
	250	RT	16900	19800
	250	RT	20400	20700
	250	175	20900	-
	250	175	19600	21300
	250	250	22200	24200
	250	250	21800	22600
	250	350	18800	23000
	250	350	22300	23000
WT	250	-100	-	-
	250	0	29800	33400
	250	0	28000	32600
	250	RT	30000	30000
	250	RT	29900	29900
	250	175	28900	30300
	250	175	28800	31900
	250	250	24000	30000
	250	250	28600	30600
	250	350	22300	29100
	250	350	19700	26300
βQ	10	RT	24300	32900
	10	RT	26400	31600
	250	RT	23600	23600
	250	RT	21400	21400
	10	200	-	53395
βQH	250	200	-	14566

Table A-11 (Ref. 15)
FRACTURE TOUGHNESS OF BETA-TREATED AND WELD-METAL ZIRCALOY-4:
ROOM TEMPERATURE-TRANSGRANULAR FRACTURES

H (μg/g)	Fluence (10^{24} n/m^2)	K_{IC} MPa$\sqrt{m}$
10	10.4	43.9
46	10.3	33.3
240	47.0	27.6
240	47.0	28 5
240	47.0	28.2
240	47 0	31.1
240	47.0	25.6
240	47.0	27.7
246	0.0	26.7
247	28.8	22.4
250	10.1	26.7
250	20 4	27.1
250	0.0	23.5
250	0.0	26.0
262	10.3	26.2
267	0.0	25.1
296	0.0	24.5
300	0.0	24.2
400	0.0	21.8
401	0 0	20.1
405	29.9	21.2
411	0 0	20 1
462	28 3	21 5
465	28 2	20 0
483	12 8	18 4
498	27.8	22.0
500	28.9	19.4
500	0.0	16.5
500	0.0	19.1
500	0.0	18.2
521	0.0	20.6
526	0.0	20.2
531	28.5	19.1
559	0.0	20.9
579	0.0	18.3
1200	0.0	18.2
1275	0 0	15 1
1278	0 0	16.6
1449	29.9	16.2
1558	30.8	16 8
1647	12.8	13.5

Table A-12 (Ref. 15)
FRACTURE TOUGHNESS OF BETA-TREATED AND WELD-METAL ZIRCALOY-4: ROOM TEMPERATURE-INTERGRANULAR FRACTURES

H (μg/g)	Fluence (10^{24} n/m^2)	K_{IC} MPa$\sqrt{m}$
668	0.0	14.8
707	0.0	12.4
950	0.0	13.1
1012	28.6	15.8
1485	28.6	13.0
1830	0.0	11.2
2225	0.0	17.8
2540	0.0	15.1
4000	0.0	7.4

Table A-13 (Ref. 15)
FRACTURE TOUGHNESS OF BETA-TREATED AND WELD-METAL ZIRCALOY-4: ELEVATED TEMPERATURE-TRANSGRANULAR FRACTURES

Temperature (°C)	H (μg/g)	Fluence (10^{24} n/m^2)	K_{IC} MPa$\sqrt{m}$
149	240	53.0	34.5
149	253	10.3	31.2
149	253	29.3	29.3
149	453	26.6	21.5
149	494	28.6	21.7
149	505	28.5	22.4
177	446	64.0	20.7
177	1337	64.0	21.3
204	489	12.8	24.5
204	586	12.8	23.0
204	1606	12.8	13.3
260	237	14.0	46.9
260	441	14.0	33.9
260	446	14.0	27.1

Table A-14 (Ref. 15)
FRACTURE TOUGHNESS OF BETA-TREATED AND WELD-METAL ZIRCALOY-4: ELEVATED TEMPERATURE-INTERGRANULAR FRACTURES

Temperature (°C)	H (μg/g)	Fluence (10^{24} n/m^2)	K_{IC} MPa$\sqrt{m}$
149	1620	27.7	13.8
149	1825	27.7	11.3
149	2197	27.7	14.6
149	3192	27.7	12.3

Table A-15 (Ref. 15)
FRACTURE TOUGHNESS OF ALPHA-ANNEALED ZIRCALOY-4: TRANSGRANULAR FRACTURES

Temperature (°C)	H (μg/g)	Fluence (10^{24} n/m^2)	K_{IC} MPa$\sqrt{m}$
29	40	150	37.2
29	40	150	35.8
29	40	150	46.3
149	40	150	54.5
204	40	150	61.2
204	40	150	57.3
204	40	150	48.7
260	40	150	56.1

Table A-16 (Ref. 16)
PL TENSION TEST RESULTS FOR ANNEALED AND COLD-WORKED ZIRCALOY-2 CLADDING

Test Temp. (K)	W mm	J_{max} kN/m	J_{pl} kN/m	J_{el} kN/m
293	15	-	-	-
	15	218	181	-
	15	203	175.5	27.5
573	25	132	115.5	16.5
	15	-	-	-
	15	146	129	17
	15	-	-	-
293	15	-	-	-
	25	-	-	-
	25	-	-	-
	25	-	-	-
	25	91	45	46
	25	101.5	53	48.5
	25	88.5	42.5	46
	15	99	44.5	54.5
573	25	-	-	-
	25	105	73	32
	15	128	83	45
	15	103	70	33

A-19

Table A-17 (Ref. 16)
PL TENSION TEST RESULTS FOR HYDRIDED CORROSION SPECIMENS

Test Temp. (K)		W mm	J_{max} kN/m	J_{pl} kN/m	J_{el} kN/m
293		25	97.5	61.5	36
	573	15	105	81.5	23.5
293		15	111	71.5	39.5
	573	15	140	115.5	24.5
293		25	108.5	77.5	31
		15	-	-	-
293		25	63	32.5	30.5
		25	-	-	-
	573	25	103.5	91	12.5
293		25	68	40	28
	573	15	139.5	120.5	19
293		15	30.5	14.5	16
	573	15	150.5	126.5	24
293		25^A	-	≈0	-
	573	15	167.5	125	42.5
293		25	-	-	-
		15	72	31	41
	573	25	108	98.5	9.5
293		15	-	-	-
		25	10.5	≈0	10.5

A The specimen was broken when placed into testing machine.

About EPRI

EPRI creates science and technology solutions for the global energy and energy services industry. U.S. electric utilities established the Electric Power Research Institute in 1973 as a nonprofit research consortium for the benefit of utility members, their customers, and society. Now known simply as EPRI, the company provides a wide range of innovative products and services to more than 1000 energy-related organizations in 40 countries. EPRI's multidisciplinary team of scientists and engineers draws on a worldwide network of technical and business expertise to help solve today's toughest energy and environmental problems.

EPRI. Electrify the World